Provided for non-commercial research and education use.
Not for reproduction, distribution or commercial use.

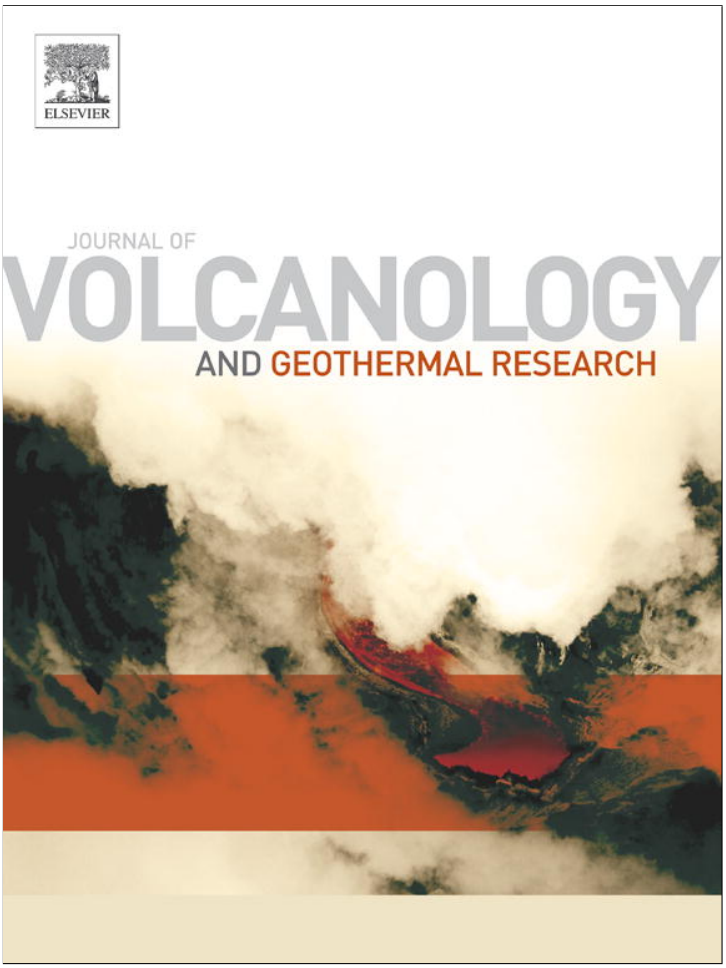

(This is a sample cover image for this issue. The actual cover is not yet available at this time.)

This article appeared in a journal published by Elsevier. The attached copy is furnished to the author for internal non-commercial research and education use, including for instruction at the authors institution and sharing with colleagues.

Other uses, including reproduction and distribution, or selling or licensing copies, or posting to personal, institutional or third party websites are prohibited.

In most cases authors are permitted to post their version of the article (e.g. in Word or Tex form) to their personal website or institutional repository. Authors requiring further information regarding Elsevier's archiving and manuscript policies are encouraged to visit:

http://www.elsevier.com/copyright

Author's personal copy

Journal of Volcanology and Geothermal Research 243-244 (2012) 69–80

Contents lists available at SciVerse ScienceDirect

Journal of Volcanology and Geothermal Research

journal homepage: www.elsevier.com/locate/jvolgeores

The Upper and Lower Nisyros Pumices: Revisions to the Mediterranean tephrostratigraphic record based on micron-beam glass geochemistry

E.L. Tomlinson [a,*], H.S. Kinvig [b], V.C. Smith [c], J.D. Blundy [b], J. Gottsmann [b], W. Müller [a], M.A. Menzies [a]

[a] Department of Earth Sciences, Royal Holloway University of London, Egham, UK
[b] Department of Earth Sciences, University of Bristol, Bristol, UK
[c] Research Laboratory for Archaeology and the History of Art, University of Oxford, Oxford, UK

ARTICLE INFO

Article history:
Received 14 November 2011
Accepted 8 July 2012
Available online 17 July 2012

Keywords:
Tephra
Tephrochronology
Nisyros
Trace element
Volcanic glass

ABSTRACT

The Greek island of Nisyros is the source of tephra found in distal settings throughout the Aegean. In this contribution, we define geochemical fingerprints for the Lower and Upper Pumice eruptions of Nisyros based on micron-beam major (EMPA) and trace (LA-ICP-MS) element data. These two eruptions are compositionally distinct from each other. The high phenocryst content of proximal Lower and Upper Pumice tephra means that the differences between the two magmas are masked in whole-rock analyses. We demonstrate that all previous reports of distal marine and continental tephras correspond to the younger Upper Pumice *not* the older Lower Pumice. This has important implications for the marine tephrochronology of the Mediterranean and for the age of the Upper and Lower Pumice eruptions. We suggest an age of at least 47 ka for the Upper Pumice and an older, unconstrained age for the Lower Pumice.

© 2012 Elsevier B.V. All rights reserved.

1. Introduction

Tephra layers are recognized as a fundamental tool for correlating between distal sedimentary archives, such as marine, lacustrine and terrestrial cores (tephrostratigraphy) (e.g. Keller et al., 1978; Paterne et al., 1988; Wulf et al., 2004). In addition, if the age of the source eruption is known, tephra layers represent an independent tool for dating sedimentary records (tephrochronology). Tephrochronology is particularly valuable for dating sedimentary sequences older than the ~50 ka limit of radiocarbon dating and for applications where the required precision is better than the millennial scale offered by the radiocarbon system (Lowe et al., 2007). Accurate dating and correlation between different sedimentary records is required for applications such as establishing the rate of abrupt environmental transitions, for investigating links between changes in sedimentation rate and paleoclimatic events and for modelling the rate of sediment influx in marine basins.

The Greek island of Nisyros is a Quaternary stratovolcano, which formed during repeated cycles of effusive and explosive eruptions of calc-alkaline basaltic-andesitic to rhyolitic lavas and pyroclastics (Di Paola, 1974; Limburg and Varekamp, 1991). The caldera is associated with two major Plinian eruptions: the Lower Pumice and the Upper Pumice (Di Paola, 1974; Limburg and Varekamp, 1991; Volentik et al., 2002; Buettner et al., 2005; Francalanci et al., 2005). Tephra from Nisyros has been identified in several marine and terrestrial cores from the Eastern Mediterranean (Vinci, 1985; Hardiman, 1999; Margari et al., 2007; Aksu et al., 2008). The delta tephra (Aksu et al., 2008) and Nisyros Ash (Hardiman, 1999) from Aegean marine cores, and the ML-3 tephra from the Greek island of Lesvos (Margari et al., 2007) have previously been correlated with the Lower Pumice. The Lesvos terrestrial core also preserves a second Nisyros tephra, ML-4, which has been correlated with the Upper Pumice on the basis of its stratigraphic position above ML-3 (Margari et al., 2007).

Tephrochronology requires that the age of the source eruption is known. Determined ages for the Upper and Lower Pumice eruptions of Nisyros range from 29 to 110 ka (Fig. 1). The Upper Pumice is stratigraphically overlain by the ca. 31 ka BP Yali-2/Yali-C layer on Nisyros (Federman and Carey, 1980), placing an upper limit on the age of the Upper Pumice. Charcoal in the Upper Pumice has been radiocarbon dated at >47.7 cal ka BP (Limburg and Varekamp, 1991, calibrated using the IntCal09 calibration curve of Reimer et al., 2009). There is also a discordant age of 110 ± 40 ka age obtained by fission track analysis of volcanic glass from the Upper Pumice (Barberi et al., 1988), this age is not considered here. The Lower Pumice has not been dated. An age of 28.9 ± 0.6 cal ka BP obtained by radiocarbon dating of the palaeosol that underlies the Lower Pumice (Rehren, 1988, calibrated using the IntCal09 calibration curve of Reimer et al., 2009) is not consistent with the stratigraphic location of the Lower Pumice below the Yali-C layer (Keller et al., 1989). A series of K–Ar ages for lava flows below the Lower Pumice also give ages younger than the Upper Pumice. The discordance between published ages for the Upper and Lower Pumice and the fact that their ages are close to the upper limit of radiocarbon dating, means that their ages are poorly constrained. Additional age information may be provided by importing the ages of correlated distal tephra, assuming that the

* Corresponding author.
E-mail address: e.tomlinson@es.rhul.ac.uk (E.L. Tomlinson).

0377-0273/$ – see front matter © 2012 Elsevier B.V. All rights reserved.
doi:10.1016/j.jvolgeores.2012.07.004

Author's personal copy

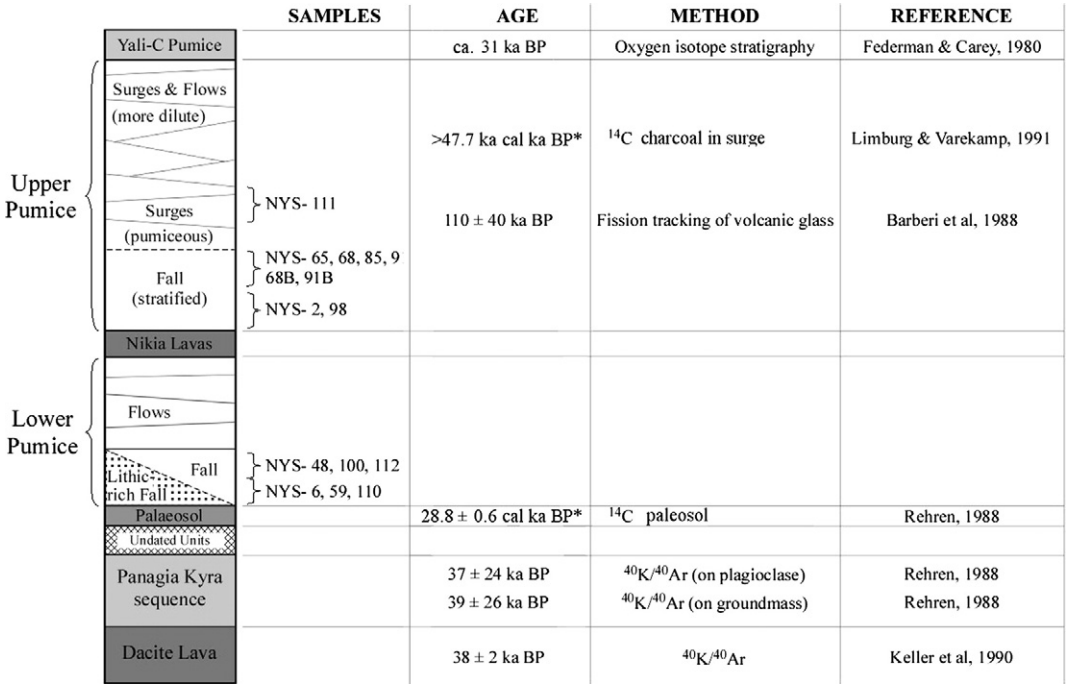

Fig. 1. Simplified stratigraphic log of Nisyros proximal units showing sampled units. Also shown are determined ages for various units from the literature, *radiocarbon ages have been calibrated using the IntCal09 internationally accepted calibration curve (Reimer et al., 2009) at 2σ. Year 0 is 1950 AD, please see references for uncalibrated radiocarbon determinations.

proximal–distal correlation is robust. Marine cores from the Aegean give an age ca. 35 ka BP (Hardiman, 1996) for the Nisyros Ash, based on linear extrapolation of sedimentation rate. Based on oxygen isotope stratigraphy, Aksu et al. (2008) assigned an age of 42–44 Ma to the delta tephra. Radiocarbon age modelling of the terrestrial sequence on the Greek Island of Lesvos give ages of 46.8 ± 5.7 cal ka BP and 46 ± 5.7 cal ka BP for the ML-4 and ML-3 Nisyros tephras, respectively (Margari et al., 2007).

In this contribution, we provide a new micron-beam dataset for the major and trace element composition of proximal Lower and Upper Pumice rhyolite glasses. We re-assess distal occurrences of the Nisyros tephra and reassess the assigned proximal–distal correlations, with implications for our understanding of the eruptive history of Nisyros. The reassigned proximal–distal tephra correlations presented here provide constraints on the ages of the Upper and Lower Pumice eruptions, with implications for climatic reconstructions of the Aegean.

2. Regional setting

Nisyros stratovolcano lies at the eastern edge of the South Aegean Volcanic arc (Fig. 2). Volcanism in this area is the result of the northerly subduction of the African plate beneath the Aegean–Anatolian plates, resulting in the formation of numerous Late Quaternary volcanoes (Pichon and Angelier, 1979), namely Methana, Aegina, Milos, Santorini and the Kos-Yali-Nisyros volcanic field. The Kos-Yali-Nisyros volcanic centre has been active for at least 3 million years (Bachmann et al., 2010). The Nisyros caldera is thought to have developed on the edge of a larger submarine caldera formed during the 161 ka eruption of the Kos Plateau Tuff (Smith et al., 1996).

The Nisyros volcanic edifice was formed during two main eruptive cycles, which are described in detail in Limburg and Varekamp (1991), Hardiman (1999), Volentik et al. (2002) and Francalanci et al. (2005). In the first cycle, submarine eruption of basaltic–andesitic pillow lavas and hyaloclastites formed a structure that eventually emerged above sea level. The stratovolcano then developed during alternating episodes of effusive and explosive activity producing lava flows, domes and pyroclastic deposits ranging from basaltic–andesite to rhyolite. The stratovolcano was destroyed during the two major-caldera forming eruptions of the Lower Pumice and Upper Pumice at the start of the second cycle. Proximal deposits of the Lower Pumice and Upper Pumice are separated by the Nikia lavas (Hardiman, 1999). There is currently ambiguity as to which eruption generated the present-day caldera. Volentik et al. (2002) attribute the caldera depression to the Lower Pumice eruption, however most authors attribute the collapse to the Upper Pumice eruption. Francalanci et al. (1995) propose that both the Lower and Upper Pumice eruptions generated a caldera each, while an incremental collapse, contributed to by both eruptions, is suggested by Hardiman (1999). It should be noted that the Upper and Lower Pumice eruptions are described as a single 'caldera-forming unit' in some older publications (Di Paola, 1974; Wyers and Barton, 1989; St.Seymour and Vlassopoulos, 1992). Subsequent extrusions of dacitic lava have partially re-filled the main caldera. Historically, there have been 13 phreatic eruptions in the caldera, most recently during 1871–1873 and in 1888 (Marini et al., 1993). Intense hydrothermal activity and periodic unrest continues to the present day (Caliro et al., 2005; Lagios et al., 2005; Gottsmann et al., 2007).

Both the Lower Pumice and Upper Pumice eruptions were characterized by low magnitude phreatomagmatic explosions (Hardiman, 1999). Lower Pumice deposits comprise pumice fall followed by pyroclastic density currents and lithic lag breccias (Hardiman, 1999; Volentik et al., 2002). Isopach mapping indicates dispersal towards the NE (Hardiman, 1999) or NNE (Longchamp et al., 2011). Estimates of the volume of erupted magma vary from >0.3 km^3 (Hardiman, 1999) and 0.2 km^3 calculated by extrapolation of isopach lines, to 2.7 km^3 from an inversion method (Longchamp et al., 2011). Deposits of the Upper Pumice were laid down during a fall phase followed by surge, breccia and pyroclastic density currents (Limburg and Varekamp, 1991; St.Seymour and Vlassopoulos, 1992). The Upper Pumice produced >0.05 km^3 (Hardiman, 1999) or 0.1–0.5 km^3 (Longchamp et al., 2011), while Limburg and Varekamp (1991) estimate a volume of 2–3 km^3 using proximal deposit thickness and the 7 cm Nisyros ash layer from a core 120 km from Nisyros (Vinci,

Author's personal copy

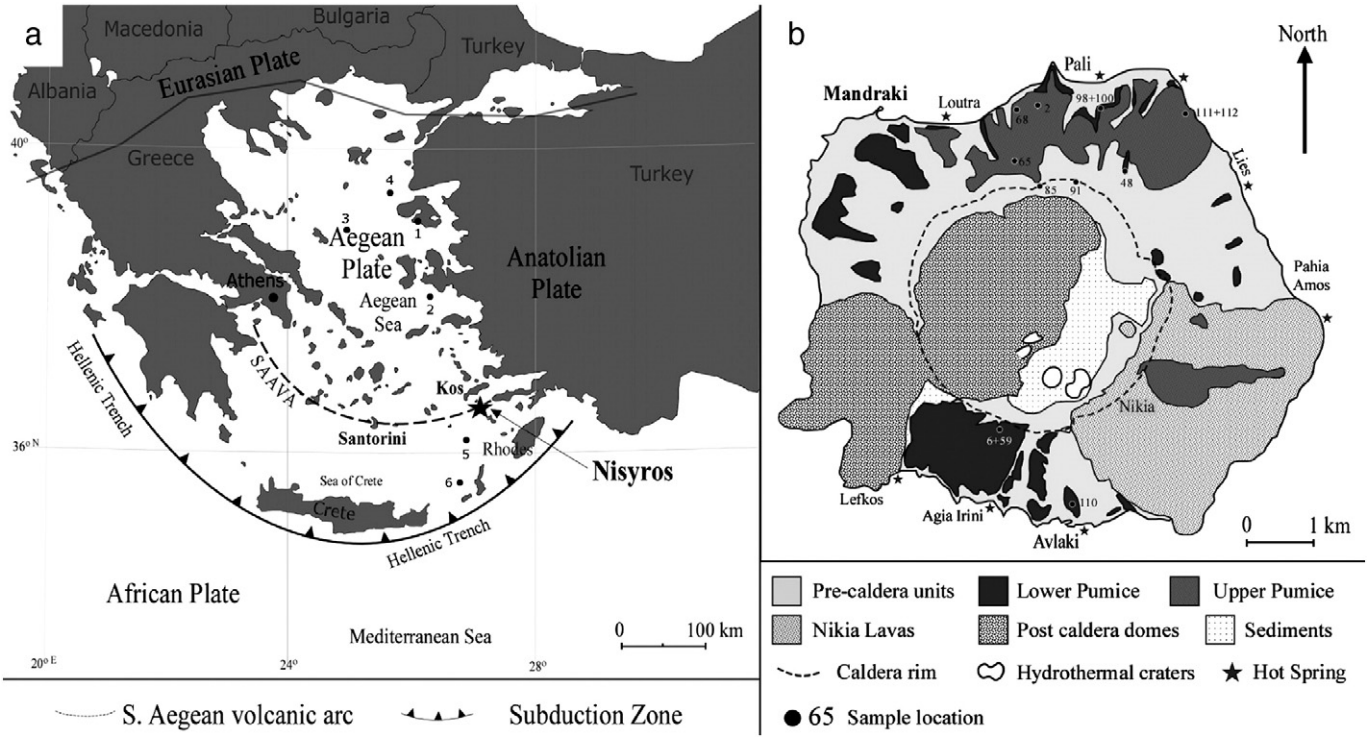

Fig. 2. a) Map of the Aegean showing location of the Nisyros volcano at the eastern end of the Aegean arc and relative to the Hellenic trench (Kinvig, 2012, unpublished Ph.D). Also shown are locations of distal cores 1 — Lesvos core, ML01 (Margari et al., 2007), 2 — MAR03-02, 3 — MAR03-28 and 4 — MAR03-49 (Aksu et al., 2008), 5 — TR172-26 (Hardiman, 1999) and 6 — MC27 (Vinci, 1985); and b) simplified geological map of Nisyros showing sample locations in the Upper and Lower Pumice.

1985). Upper Pumice tephra was dispersed to the NNE (Hardiman, 1999) or N (Longchamp et al., 2011). Both the Lower and Upper Pumice tephra were deposited from eruption columns of similar height (15 km) and are comparable in terms of proximal grainsize distribution (Longchamp et al., 2011). Volume estimates imply that the Lower Pumice was the larger event, however the estimates for the two eruptions are based on limited proximal exposure and overlap, furthermore the models of Longchamp et al. (2011) only consider the fall components of each eruption from the NE of the island and do not include the pyroclastic density currents.

3. Materials and methods

3.1. Samples

Pumice samples were collected from both the Lower Pumice and Upper Pumice deposits on the island of Nisyros (Figs. 1,2).

Lower Pumice samples were collected from fall deposits. Samples NYS-6, 59, and NYS-110 were collected from a coarse, creamy-white, pumice fall deposit on the southern flank of Nisyros. The samples contain up to 50% lithic clasts, including ancestral lavas, basement sediments and skarns and igneous intrusives (Hardiman, 1999). These are interpreted as representing a combination of fall deposits and lithic lag breccias, with the most proximal deposits representing both and the more distal units being just fallout. Samples NYS-100, NYS112 were collected from fall deposits in the north of Nisyros, which consist of fairly well-sorted to crudely stratified pumice clasts with no grading. Sample NYS-48 was collected from a bright white lapilli fall unit in the north of Nisyros, which had experienced some remobilisation. Lithic content in the northern fall units is far lower than that of the southern outcrops (<15%).

Upper Pumice samples were collected from fall and pumiceous surge deposits from the north and north-east of Nisyros. Samples NYS-65, NYS-68, NYS-85 and NYS-91 were collected from crudely to well-stratified pumice fall units, which show transitions to pumiceous surges in their upper parts. Samples NYS-2 and NYS-98 are from crudely stratified pumice fall deposits, and sample NYS-111 was collected from pumice-rich surge deposits in the northeast. The Upper Pumice outcrops are bright white in appearance, and generally lithic-poor with just <10–15%, excepting the pyroclastic flows, which contain lenses of lithic-lag breccia.

Vesicularity and bubble wall thickness of the pumice clasts varies significantly (Fig. 3a–c), but overall the Lower Pumice falls generally exhibit greater vesicularity with larger bubbles, while the Upper Pumice clasts in the fallout and pumice-rich surges generally exhibit very small vesicles. Both the Lower Pumice (5–10 vol.% crystals) and Upper Pumice (15–20 vol.% crystals) are phenocryst-rich. Plagioclase feldspar, clinopyroxene and orthopyroxene are the dominant phenocryst phases in both the Lower and Upper Pumice. Clinopyroxene is more common than orthopyroxene and both frequently have inclusions of Fe–Ti oxides. Minor amphibole, zircon and apatite also occur. The groundmass is micro-phenocryst and microlite free (Fig. 3d).

Some workers report the presence of a paleosol between the Lower and Upper Pumice (e.g. Longchamp et al., 2011), however we did not find evidence of a paleosol. In places there is a fine ash layer which has altered in parts to an orange colour, but laterally it then transitions into the pure white colour expected of ash. The layer also lacks non-crystalline minerals, except for amorphous silica, so cannot be classified as an andisol (Drouza et al., 2006).

3.2. Analytical methods

Micron-scale major and trace element analyses were undertaken on the same glass samples by electron-microprobe analysis (EMPA) and laser-ablation inductively coupled plasma mass spectrometry (LA-ICP-MS).

Author's personal copy

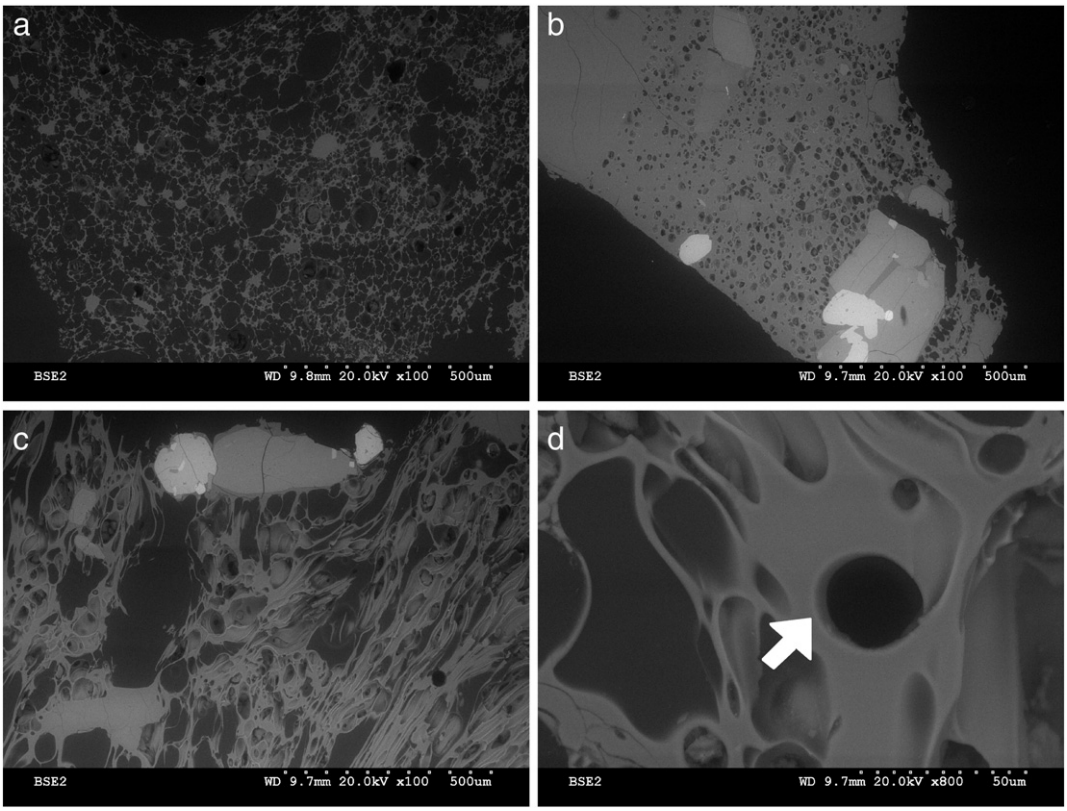

Fig. 3. Backscatter electron images of typical Nisyros Pumice: a) highly expanded Upper Pumice; b) low vescicularity Upper Pumice; c) phenocryst-rich Upper Pumice sample with euhedral and subhedral plagioclase and clinopyroxene both with oxide inclusions; and d) microcryst and microlite free groundmass glass; the circular feature indicated by the arrow is a 34 μm laser ablation pit.

3.2.1. Electron micro-probe analysis (EMPA)

Major element compositions were determined using JEOL8600 electron microprobe, equipped with 4 spectrometers and SamX software, at the Research Laboratory for Archaeology and the History of Art, University of Oxford. An accelerating voltage of 15 kV, low beam current (6 nA), and defocused (10 μm) beam were used to minimize Na migration. Count times were 30 s on each peak, except for Na (10 s), P and Cl (60 s). The instrument was calibrated for each set of beam conditions using a suite of appropriate mineral standards. The calibration was verified using a range of secondary glass standards from the Max Planck Institute. Secondary glass (MPI-DING suite; Jochum et al., 2006) and mineral (Smithsonian Institute) standards were analysed between and within runs. The PAP absorption correction method was used. Three replicate analyses were made on each sample and analyses with totals of <94% were discarded. Analyses with totals >94% are considered acceptable because loss on ignition analysis of whole rock samples gives values of <6% (Table 2). Sample totals are normalised to 100 wt.% in all plots and tables. Accuracies of analyses of the MPI-DING glasses are <5% for concentrations >0.8 wt.%, in the Nisyros glasses this includes SiO_2, Al_2O_3, FeO, CaO, Na_2O, K_2O; analytes with concentrations <0.2 wt.% are significantly less accurate, this includes TiO_2, MnO, MgO, P_2O_5 and Cl in the Nisyros glasses. Reproducibility is <10% relative standard deviation (%RSD) for analytes with concentrations >0.8 wt.%. Error bars on plots represent the 2σ of replicate analyses of MPI-DING ATHO-G.

3.2.2. Laser ablation inductively coupled plasma mass spectrometry (LA-ICP-MS)

LA-ICP-MS analyses of proximal tephra samples were performed using an Agilent 7500es coupled to a Resonetics 193 nm ArF excimer laser-ablation system (RESOlution M-50 prototype) with a two-volume ablation cell (Müller et al., 2009) at the Department of Earth Sciences, Royal Holloway University of London. We used a 34 μm spot size, depending on the size of the area available for analysis in different samples. Fig. 3d shows typical laser ablation pit in Nisyros pumice, with sharp crater walls and a symmetrical morphology. The repetition rate was 5 Hz and the count time was 40 s (200 pulses) on the sample and 40 s on the gas blank (background). Concentrations were calibrated using NIST612 with ^{29}Si as the internal standard. Data reduction was performed manually using Microsoft Excel. Full details of the analytical and data reduction methods are given in Tomlinson et al. (2010). Accuracies of analyses of ATHO-G and StHs6/80-G MPI-DING glass analyses are typically <5%. For consistency with EMPA error reporting, reproducibility of ATHO-G analyses is <6% RSD% and error bars on plots represent the 2σ the standard deviation of replicate analyses of ATHO-G. Relative standard errors (RSE%) for tephra LA-ICP-MS analyses are typically <2% %RSD for Rb, Sr, Y, Zr, Nb, Ba, La, Ce, <4% for Pr, Nd, Th, U and 4–8% for Sm, Eu, Gd, Dy, Er, Yb, Lu, Ta.

3.2.3. X-ray fluorescence (XRF)

Whole rock XRF analyses of individual pumice clasts were performed at Leicester University using a PANalytical Axios Advanced PW4400 XRF spectrometer. Major elements were determined on fused glass beads prepared from ignited sample powders using a 5:1 mix of lithium metaborate and lithium tetraborate flux. Accuracies of major element analyses are <3% at >1 wt.% and <10% at >0.5 wt.%. Trace elements were analysed on pressed powder pellets prepared with 7% PVA solution, accuracies are <5% at >20 ppm. Analytical precision is typically <5%RSD at >1 wt.% and >20 ppm.

4. Results

Representative major and trace element glass data are given in Table 1, the full dataset is available as supplementary data.

Author's personal copy

Table 1
Representative micron-beam major (EMPA; wt.%) and trace (LA-ICP-MS; ppm) element data for Lower Pumice and Upper Pumice glasses. Major element compositions are normalised to 100%, the un-normalised total is given. Sample numbers show sample name-clast number e.g. NYS2-2.

Sample	Lower Pumice					Upper Pumice							
	NYS 112-4	NYS 100-2	NYS 110-2	NYS 6,59-2	NYS 48-3	NYS 2-2	NYS 68-1	NYS 65-2	NYS 91-1	NYS 85-3	NYS 98-4	NYS 111-5	NYS-91bomb-8
Total	96.28	96.77	95.73	97.47	96.43	95.04	96.22	96.88	95.55	96.79	96.39	97.44	95.98
SiO_2	76.27	76.08	76.05	76.13	76.16	76.80	76.83	77.32	76.99	77.29	77.44	77.55	75.63
TiO_2	0.27	0.26	0.26	0.30	0.24	0.22	0.23	0.21	0.24	0.24	0.22	0.22	0.35
Al_2O_3	12.76	13.10	12.85	12.86	12.83	12.65	12.63	12.35	12.46	12.20	12.22	11.93	12.74
MnO	0.05	0.05	0.06	0.07	0.08	0.06	0.04	0.04	0.03	0.02	0.01	0.04	0.01
MgO	0.17	0.19	0.16	0.18	0.17	0.15	0.17	0.15	0.18	0.16	0.18	0.17	0.13
FeO	1.42	1.47	1.47	1.53	1.47	1.44	1.32	1.22	1.29	1.30	1.13	1.26	1.41
CaO	0.92	0.90	0.91	0.89	0.95	0.94	0.94	0.94	0.98	0.92	0.94	0.98	0.96
Na_2O	3.52	3.69	3.75	3.76	3.67	3.24	3.33	3.28	3.25	3.26	3.24	3.29	3.74
K_2O	4.34	4.03	4.26	4.08	4.16	4.30	4.29	4.28	4.39	4.36	4.39	4.33	4.57
P_2O_5	0.05	0.03	0.03	0.05	0.04	0.00	0.00	0.01	0.01	0.04	0.02	0.03	0.04
Cl	0.21	0.19	0.20	0.17	0.21	0.19	0.23	0.20	0.20	0.22	0.21	0.20	0.41
Rb	129	132	129	134	137	144	145	146	147	152	150	152	–
Sr	91	91	82	88	84	91	93	94	101	95	95	99	–
Y	19	20	18	19	17	18	18	18	19	17	18	18	–
Zr	240	258	237	251	235	147	153	156	167	153	158	159	–
Nb	21	22	21	21	21	19	19	19	19	19	19	19	–
Ba	926	972	894	922	870	878	924	915	895	910	918	945	–
La	38	40	36	39	36	38	39	39	41	38	39	40	–
Ce	66	70	64	67	65	66	69	69	69	68	70	71	–
Pr	6.2	6.6	6.0	6.2	5.8	6.2	6.3	6.3	7.0	6.2	6.3	6.5	–
Nd	21	22	20	21	19	20	22	20	23	21	22	21	–
Sm	3.7	3.6	3.5	3.1	3.7	3.3	3.4	3.3	3.2	3.6	3.6	3.1	–
Eu	0.5	0.5	0.4	0.5	0.5	0.4	0.4	0.4	0.5	0.4	0.4	0.4	–
Gd	3.0	3.1	3.4	2.5	2.8	2.5	3.0	2.9	2.7	3.0	3.1	2.8	–
Dy	2.9	3.2	2.8	2.9	2.8	2.9	3.0	2.9	2.9	2.9	2.8	3.0	–
Er	2.0	2.2	2.1	2.1	1.8	1.8	2.0	1.9	1.9	1.8	2.0	2.0	–
Yb	2.4	2.6	2.1	2.5	2.3	2.2	2.3	2.3	2.3	2.0	2.3	2.3	–
Lu	0.4	0.4	0.4	0.4	0.3	0.3	0.3	0.3	0.4	0.3	0.4	0.4	–
Ta	1.6	1.6	1.5	1.4	1.4	1.4	1.5	1.5	1.4	1.4	1.5	1.5	–
Th	14	15	13	14	13	15	16	17	15	16	16	16	–
U	4.3	4.5	4.0	3.9	4.3	4.6	4.9	4.8	4.7	4.5	4.7	4.9	–

Lower Pumice and Upper Pumice glasses are high-K rhyolites (Le Maitre et al., 1989). Incompatible element concentrations in the glasses are elevated by 2–200× primitive mantle, with negative anomalies at Nb, Ta and also at Ba, Sr and Eu (Fig. 4), consistent with the arc setting of Nisyros and with feldspar fractionation, respectively. The Lower Pumice and Upper Pumice glasses have distinct major and trace element geochemistries. The principal differences between the Lower Pumice and Upper Pumice glasses are that the Upper Pumice has significantly higher SiO_2 and lower Al_2O_3 and Na_2O and lower, but overlapping, FeO and TiO_2 and higher but overlapping CaO and K_2O (Fig. 5). Therefore, the two tephra populations can be distinguished on the basis of major element geochemistry. The Upper Pumice is also characterized by lower Zr, Nb and to a lesser extent Y and Eu/Eu_N^* and also by higher V, Th, Rb and Sr (Fig. 6).

Lower Pumice glasses have a narrow range of SiO_2 concentrations (75.8–76.5 wt.%) and form a tight compositional range for most major elements TiO_2 (0.26 ± 0.04 wt.%), FeO (7.8 ± 0.2 wt.%), MgO (0.18 ± 0.03 wt.%), CaO (0.90 ± 0.05 wt.%) and K_2O (4.2 ± 0.2 wt.%). Concentrations of Al_2O_3 (12.7–13.3 wt.%) and Na_2O (3.4–3.9 wt.%) decrease with increasing SiO_2. Lower Pumice glasses have a narrow range of trace element concentrations (Zr = 263 ± 24; Rb 133 ± 11, Sr = 88 ± 91, Th = 13.4 ± 2.1 ppm) resulting in constant inter-element ratios such as HFSE to Th (Zr/Th = 17.7 ± 1.4, Nb/Th = 1.54 ± 0.17). Lower Pumice rhyolites have small Eu anomalies (Eu/Eu_N^* = 0.72 ± 0.10) and a gently negative REE trend (Ce/Yb_N = 1.20 ± 0.14).

The SiO_2 concentration of the Upper Pumice glasses span a narrow range (76.3–77.7 wt.% SiO_2). Concentrations of most major elements are constant: TiO_2 (0.24 ± 0.07 wt.%), MgO (0.17 ± 0.04 wt.%), CaO (0.95 ± 0.10 wt.%), Na_2O (3.3 ± 0.1 wt.%) and K_2O (4.3 ± 0.2 wt.%), while Al_2O_3 (11.9–13.1 wt.%) and FeO (7.4–7.8 wt.%) decrease with increasing SiO_2. Trace element concentrations (Zr = 153 ± 15, Rb = 149 ± 8, Sr = 93 ± 11 and Th = 15.5 ± 1.8 ppm) and ratios (Zr/Th = 9.8 ± 0.8, Nb/Th = 1.22 ± 0.11) are constant in Upper Pumice glasses, and the Upper Pumice has a small Eu anomaly (Eu/Eu_N^* = 0.63 ± 0.14) and gently negative REE trend (Ce/Yb_N = 1.31 ± 0.12).

5. Discussion

5.1. Comparison with distal tephras

Tephra recognized as originating from Nisyros has been documented in marine and continental cores up to 300 km from Nisyros. These include five Aegean marine cores (TR172-26, Hardiman, 1999; MC27, Vinci, 1985; MAR03-02, MAR03-28 and MAR03-49, Aksu et al., 2008) and a continental core from the Greek island of Lesvos (ML01; Margari et al., 2007). Cores MC27 and TR172-26 were taken from south of Nisyros, all other core locations are to the north-north-east of Nisyros. Average compositions of these distal tephras are given in Table 3. The authors used similarity coefficients (Borchardt et al., 1971; Margari et al., 2007; Aksu et al., 2008) and principal component analysis (Hardiman, 1999) to statistically compare the major element geochemistry of the distal tephra to proximal data for the Lower and Upper Pumice. On this basis, the Nisyros Ash from TR172-26 (Hardiman, 1999), the delta tephra from the three MAR03 cores (Aksu et al., 2008) and ML-4 from terrestrial core ML01 (Margari et al., 2007) were correlated to the Lower Pumice. Vinci (1985) did not specifically link the Nisyros Ash in core MC27 to either the Lower or Upper Pumices. ML-3, a second and non-contiguous Nisyros tephra layer in ML01 was linked to the Upper Pumice on the basis of stratigraphy, despite being geochemically identical to ML-3

Author's personal copy

Table 2
Major (wt.%) and (where available) trace element data (ppm) for average proximal Upper and Lower Pumice, and for distal tephra layers correlated to Nisyros (Vinci, 1985; Hardiman, 1999; Margari et al., 2007; Aksu et al., 2008). Major element concentrations are normalised to 100 wt.%, excluding MnO, P_2O_5 and Cl to facilitate comparison. Coefficients of variation (%CV) are calculated using the method of Borchardt et al. (1971). Statistical distances (D^2) are calculated using the method of Perkins et al. (1995). Note: *empa data for Margari et al., 2007 excludes analyses 1–56 due to anomalously high Na_2O in these analyses.

Reference	This study	This study	Aksu et al., 2008		Margari et al., 2007		Hardiman, 1999	Vinci, 1985
Core layer	Proximal	Proximal	M03-2	M03-28	ML01	ML01	TR172-26	MC27
	UP (2σ)	LP (2σ)	N2 (2σ)	A3 (2σ)	ML-3* (2σ)	ML-4 (2σ)	133.1–133.4 (2σ)	301–307 cm (2σ)
n	51	47	15	12	69	56	31	3
SiO_2	77.35 (0.51)	76.24 (0.26)	77.74 (0.51)	77.59 (0.45)	77.47 (0.34)	77.66 (0.32)	77.39 (1.24)	77.26 (na)
TiO_2	0.23 (0.05)	0.26 (0.04)	0.20 (0.04)	0.22 (0.05)	0.24 (0.02)	0.23 (0.02)	0.11 (0.14)	0.19 (na)
Al_2O_3	12.35 (0.42)	12.97 (0.22)	12.19 (0.30)	12.19 (0.25)	12.27 (0.18)	12.19 (0.19)	12.63 (0.52)	12.31 (na)
MgO	0.17 (0.03)	0.18 (0.03)	0.17 (0.04)	0.17 (0.05)	0.18 (0.02)	0.17 (0.02)	0.14 (0.20)	0.14 (na)
FeO	1.28 (0.18)	1.54 (0.14)	1.25 (0.16)	1.32 (0.26)	1.29 (0.15)	1.27 (0.18)	0.77 (0.24)	1.13 (na)
CaO	0.95 (0.07)	0.91 (0.05)	0.95 (0.09)	0.96 (0.11)	0.98 (0.05)	0.97 (0.04)	0.97 (0.40)	0.85 (na)
Na_2O	3.28 (0.10)	3.68 (0.25)	3.27 (0.17)	3.34 (0.15)	3.20 (0.17)	3.20 (0.18)	4.28 (1.08)	3.45 (na)
K_2O	4.35 (0.14)	4.17 (0.22)	4.23 (0.29)	4.20 (0.18)	4.37 (0.17)	4.32 (0.13)	3.71 (0.72)	4.66 (na)
%CV LP			108	106	104	105	118	111
%CV UP			102	100	99	100	112	106
D^2 LP	17	16	19	25	9	–		
D^2 UP	0.8	0.5	0.1	0.7	5.0	–		
n	27	38	13	13	Bulk	Bulk		
Rb	149 (8)	133 (11)	147 (30)	137 (17)	119	120		
Sr	93 (11)	88 (9)	93 (12)	109 (71)	105	105		
Y	18 (2)	18 (2)	21 (3)	22 (2)	18	19		
Zr	153 (15)	237 (24)	177 (28)[a]	176 (17)	144	143		
Nb	19 (1)	21 (1)	19 (2)	19 (1)	18	18		
Ba	887 (68)	897 (81)	795 (123)	834 (64)	817	810		
La	38 (3)	37 (4)	40 (6)	42 (4)	31	34		
Ce	67 (4)	65 (6)	63 (8)	65 (6)	61	61		
Pr	6.2 (0.6)	6.1 (0.7)	6.1 (0.8)	6.4 (0.7)	5.9	6.1		
Nd	21 (3)	20 (3)	21 (3)	22 (2)	19	19		
Sm	3.4 (0.6)	3.4 (0.5)	3.6 (1.0)	3.5 (0.6)	3.1	3.2		
Eu	0.42 (0.07)	0.48 (0.08)	0.38 (0.14)	0.42 (0.11)	0.37	0.39		
Gd	2.8 (0.5)	2.8 (0.4)	2.9 (0.9)	3.1 (0.4)	2.8	2.8		
Dy	2.8 (0.3)	2.8 (0.5)	3.3 (0.6)	3.4 (0.4)	2.8	2.9		
Er	1.8 (0.3)	1.9 (0.3)	2.2 (0.4)	2.3 (0.3)	1.9	1.9		
Yb	2.2 (0.3)	2.3 (0.4)	2.6 (0.6)	2.6 (0.5)	2.2	2.2		
Lu	0.34 (0.05)	0.37 (0.06)	0.40 (0.08)	0.44 (0.09)	0.37	0.37		
Ta	1.5 (0.1)	1.5 (0.2)	1.6 (0.1)	1.7 (0.2)	1.6	1.6		
Th	15 (2)	13 (2)	17 (2)	19 (2)	13	15		
U	4.5 (0.5)	4.2 (0.4)	4.0 (0.4)	4.3 (0.6)	4.0	4.0		
%CV LP			96	92	107	104		
%CV UP			94	91	105	103		
D^2 (exc. MREE-HREE) LP	2.3	1.9	–	–				
D^2 (exc. MREE-HREE) UP	1.7	1.0	–	–				
Zr/Th	9.8 (0.8)	17.7 (1.4)	10.3 (0.8)	9.4 (0.7)	10.8	9.6		
Nb/Th	1.2 (0.1)	1.5 (0.2)	1.1 (0.1)	1.0 (0.1)	1.4	1.2		
Ta/Th	0.09 (0.01)	0.11 (0.01)	0.09 (0.01)	0.09 (0.01)	0.12	0.10		
Y/Th	1.1 (0.1)	1.3 (0.1)	1.2 (0.1)	1.2 (0.1)	1.31	1.28		
Ce/Yb_N	1.31 (0.12)	1.20 (0.14)	1.03 (0.21)	1.05 (0.28)	1.19	1.18		
Eu/Eu_N^*	0.63 (0.14)	0.72 (0.10)	0.55 (0.20)	0.59 (0.16)	0.60	0.62		

[a] This value is reported as 76.5 ppm in the original publication (Aksu et al., 2008), this is due to a typographic error and the correct value is 176.5 ppm (Aksu, pers. com).

(Margari et al., 2007). In this section, we re-assess the assigned source eruption for these tephras in the light of our new major and trace element glass data.

The major element compositions of distal Nisyros tephras (the Nisyros Ash, delta tephra and ML-3/ML-4 tephras) are compared to our proximal dataset for the Upper and Lower Pumice in Fig. 5. It is clear from these plots that all the distal tephras overlap completely with the Upper Pumice and not the Lower Pumice. In particular, the distal tephras have higher SiO_2 concentrations than those found in the Lower Pumice. Where trace element data is available, the distal tephras again overlap with the Upper Pumice (Fig. 6) and can be separated from the Lower Pumice by the key ratio discriminators, Zr/Th and Nb/Th and by their larger Eu anomalies (Table 3). This includes both the ML-3 and ML-4 layers from the Lesvos core, which were originally attributed to the Upper and Lower Pumice respectively (Margari et al., 2007). Table 3 presents similarity coefficients (Borchardt et al., 1971) and statistical distance results (Perkins et al., 1995) of comparisons between the major element compositions of published distal tephras and our data for the Lower and Upper Pumice.

The similarity coefficient (CV%) is based on the average ratio of mean elemental compositions of a pair of samples, with 100% indicating an exact match (Borchardt et al., 1971). The similarity coefficients (CV%) indicate a closer match with the Upper Pumice than with the Lower Pumice for all distal tephras. The Nisyros tephras in cores MC27 (Vinci, 1985), MAR03-02, MAR03-28, MAR03-49 (Aksu et al., 2008) and ML01 (Margari et al., 2007), have the CV% values close to 100% when compared to the Upper Pumice, indicating a good correlation.

Statistical distance (D^2) is a measure of the difference between pairs of samples based on both mean and standard deviation, with values approaching 0 indicating a close match. The D^2 has a chi-squared distribution for compositionally identical samples, provided that the data are normally distributed (Perkins et al., 1995).

Author's personal copy

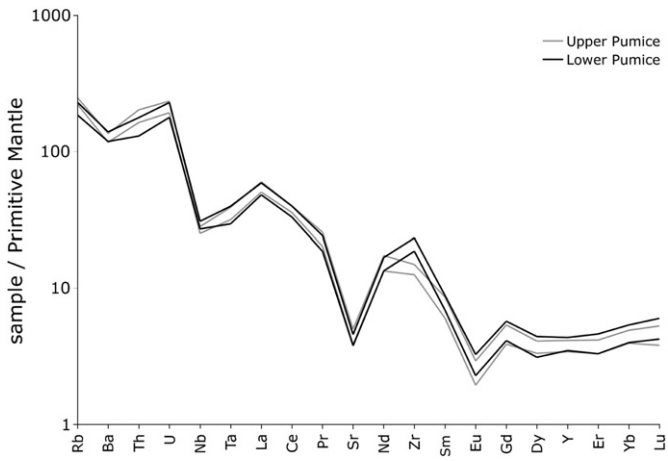

Fig. 4. Maximum and minimum incompatible trace element concentration of Upper Pumice and Lower Pumice glasses normalised to primitive mantle (Sun and McDonough, 1989).

Statistical distance analysis indicates that we can exclude a correlation between the distal tephra layers and the Lower Pumice at a confidence level of 95% ($D^2_{critical} = 15.5$). When compared to the Upper Pumice, calculated D^2 values for most distal tephras are <1. This supports a correlation between the distal Nisyros ash layers in cores MC27 (Vinci, 1985), MAR03-02, MAR03-28, MAR03-49 (Aksu et al., 2008) and ML01 (Margari et al., 2007) and the Upper Pumice, not the Lower Pumice.

The Nisyros Ash data from core TR172-26 (Hardiman, 1999) have low FeO and TiO_2, high Na_2O and $Na_2O > K_2O$, this is the reverse of what is seen in both proximal and distal data for the Nisyros glass. This is reflected in lower degrees of confidence when correlating the Nisyros ash to proximal Nisyros glasses (CV% > 110% and $D^2 > 5$). This suggests that the Nisyros Ash tephra layer in marine core TR172-26 may not be from Nisyros, or alternatively this discrepancy may be a result of poor analyses and/or the analysis of altered material.

On the basis of geochemical (concentration and ratio) and statistical considerations, we suggest that distal Nisyros ash layers in cores MC27 (Vinci, 1985), MAR03-02, MAR03-28, MAR03-49 (Aksu et al., 2008) and ML01 (Margari et al., 2007), were produced during the eruption of the Upper Pumice of Nisyros. The origin of the tephra identified as the Nisyros Ash in TR172-26 (Hardiman, 1999) is uncertain.

The next question to address is why these tephras were erroneously correlated with the Lower Pumice in their original publications. These studies compare the distal tephras to proximal tephra and rely heavily on proximal major element glass compositions reported by Hardiman (1999). Hardiman (1999) show that the SiO_2 concentration of the Upper Pumice (76.21–77.37 wt.% SiO_2) is higher than the Lower Pumice (74.61–76.63 wt.%), and our data are in agreement. However due to an unfortunate error in Table 1 of Hardiman (1999), the stated SiO_2 mean (75.5 wt.%) is lower than the stated minimum for the Upper Pumice and it is this average composition which has been commonly used for proximal–distal correlations. Furthermore, the data of Hardiman (1999) indicate that the Upper Pumice has $Na_2O < K_2O$ and the Lower Pumice has $Na_2O > K_2O$. However this is contrary to the proximal data from our study and the data presented by Francalanci et al. (1995), which indicate that both the Lower and Upper Pumice have

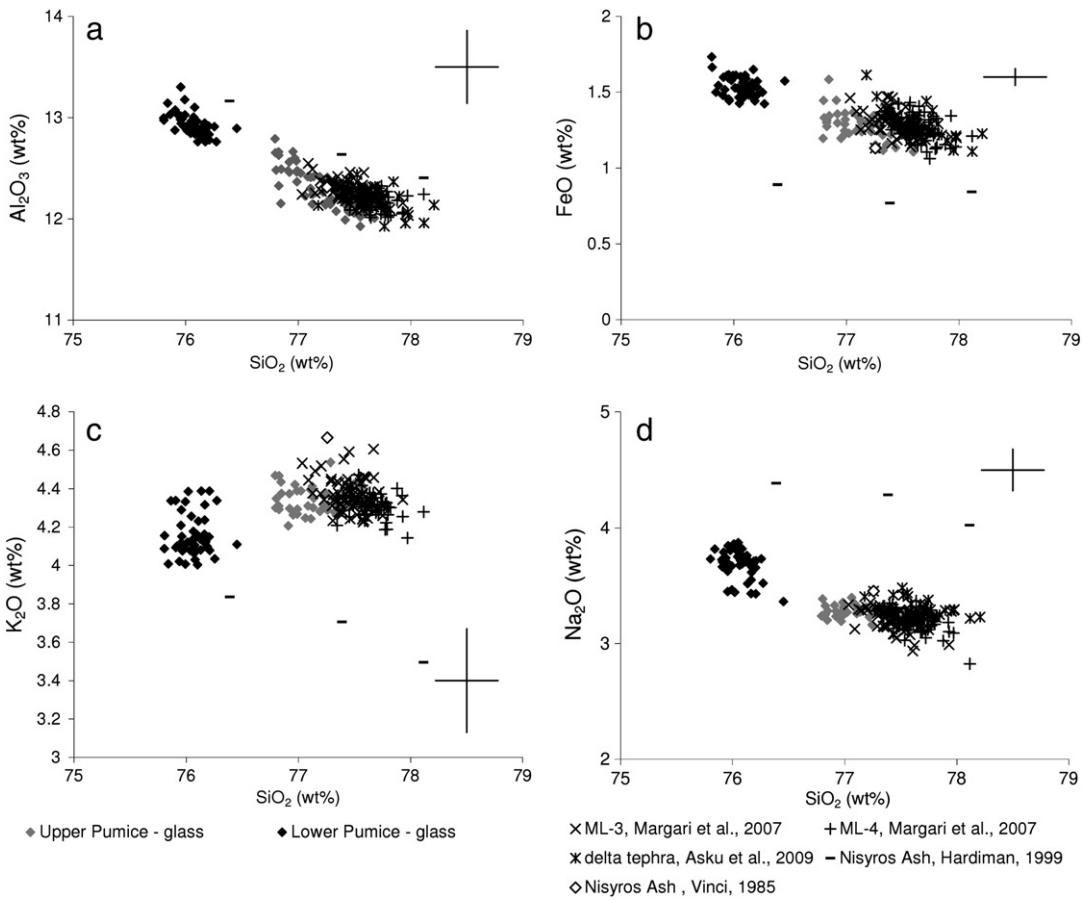

Fig. 5. Major element biplots showing Upper Pumice (grey) and Lower Pumice (black) glasses; error bars represent the 2× the standard deviation of replicate analyses of ATHO-G. Distal tephra from the Aegean (Vinci, 1985; Hardiman, 1999; Aksu et al., 2008) and the island of Lesvos (Margari et al., 2007) and attributed to Nisyros are also shown.

Author's personal copy

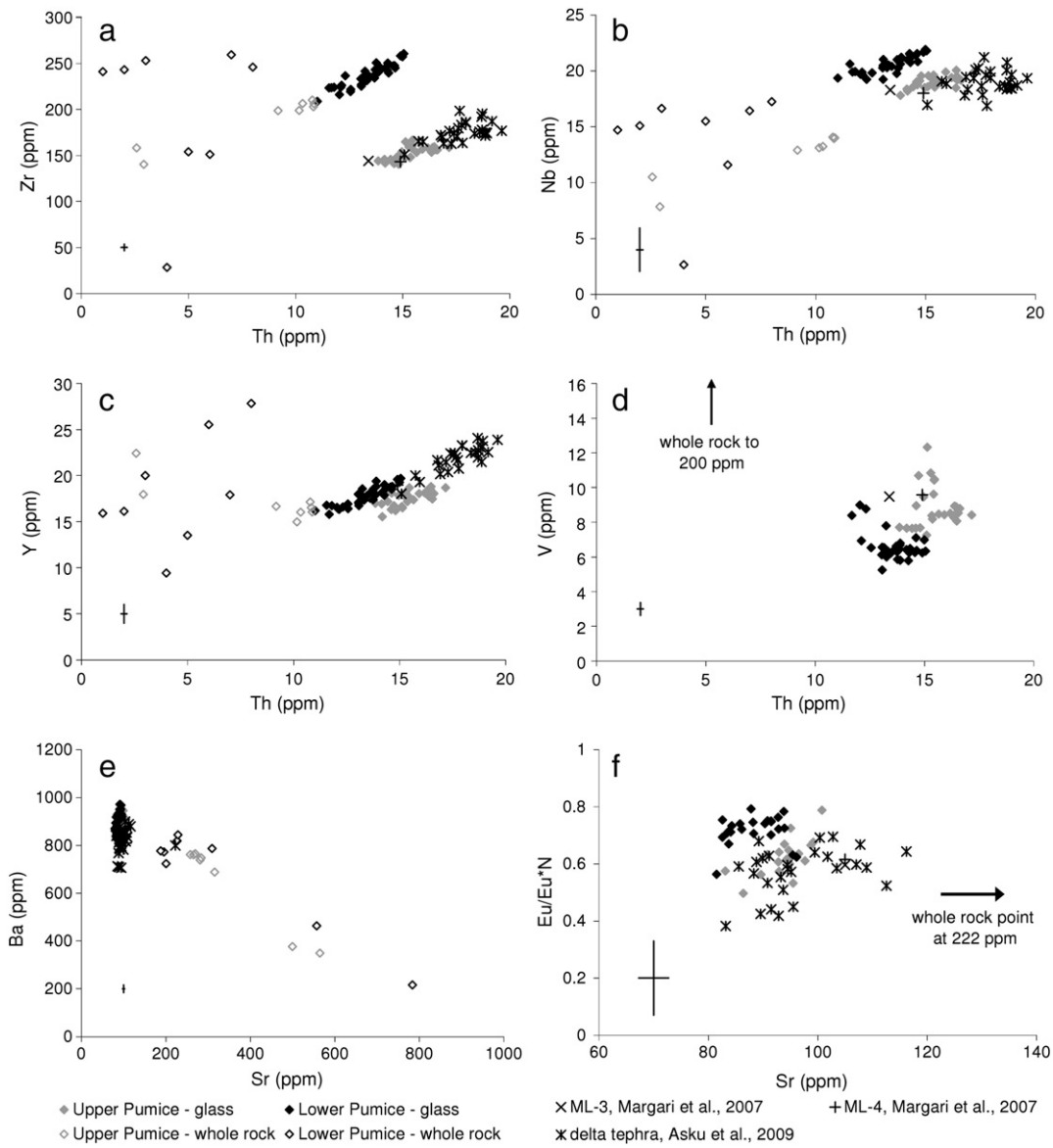

Fig. 6. Trace element biplots showing glass (solid symbols) and whole rock (open symbols) for Upper and Lower Pumice samples. Error bars represent the 2× the standard deviation of replicate analyses of ATHO-G. Distal tephra from the Aegean (Aksu et al., 2008) and the island of Lesvos (Margari et al., 2007) and attributed to Nisyros are also shown.

$Na_2O > K_2O$. This difference may be due to poor data and/or analytical error since that the data of Hardiman (1999) include analyses with totals as low as 3 wt.% and the stated errors are relatively large. Margari et al. (2007) noted that the ML-3 tephra is most similar to the Upper Pumice data of Francalanci et al. (1995). Despite this, they chose to link ML-3 to the Lower Pumice on the basis of a comparison with the data of Hardiman (1999) and on the basis of stratigraphy, since the ML-4 tephra layer from Nisyros lies higher up in the same core.

5.2. Glass 'vs' bulk analysis

More recently, some authors have used trace element data to discriminate between potential source eruptions of Nisyros (Margari et al., 2007; Aksu et al., 2008). Our study shows that the micron-beam glass trace element discriminators Zr and Nb provide the clearest separation between Nisyros Lower and Upper Pumice tephra. Numerous authors have presented whole rock trace element data for the Lower and Upper Pumice of Nisyros using XRF (St.Seymour and Vlassopoulos, 1992; Vanderkluysen et al., 2005; Zellmer and Turner, 2007) ICP-MS (Buettner et al., 2005; Margari et al., 2007) and INAA (Francalanci et al., 1995; Peltz et al., 1999; Saminger et al., 2000; Zellmer and Turner, 2007). There are no micron-beam glass trace element data in the literature. Fig. 7 shows whole rock data from the literature and this study and published data for the delta tephra (Aksu et al., 2008) and the ML-3/ML-4 tephra (Margari et al., 2007). The plots show that it is not possible to (a) separate the Lower and Upper Pumice; or (b) identify which of two Nisyros eruptions studied was the source of the distal delta or ML-3/ML-4 tephra using whole rock data. There are two main problems with the use of proximal whole rock data for proximal–distal tephrostratigraphic correlations:

(1) Whole rock geochemical data represents the average of both melt and phenocrysts and in some cases also lithic fragments.
(2) Whole rock analyses mask the extent of compositional variation within a sample. This may mean that samples are homogenised, either at the scale of a single clast in the case of mingled samples, or when several clasts are bulked together for analysis. Alternatively, apparent heterogeneity may be introduced as a result of the inclusion of variable proportions of phenocrysts.

Author's personal copy

Table 3
Whole rock major (wt.%) and trace element data (ppm), determined using XRF, for Lower Pumice and Upper Pumice samples used in this study. Major element compositions are normalised to 100%, the un-normalised total is given.

Sample	Lower Pumice					Upper Pumice						
	NYS 112	NYS 100	NYS 110A	NYS 6A	NYS 59A	NYS 2A	NYS 68A	NYS 65	NYS 91A	NYS 85	NYS 98	NYS 91bomb
SiO_2	71.58	72.75	70.68	72.58	72.24	68.52	70.12	70.04	70.54	70.78	70.50	57.40
TiO_2	0.32	0.33	0.36	0.28	0.33	0.41	0.33	0.36	0.34	0.35	0.36	0.93
Al_2O_3	13.62	14.16	15.30	14.36	14.29	15.45	15.18	15.16	15.07	14.96	15.15	18.49
MnO	0.07	0.07	0.07	0.07	0.07	0.07	0.06	0.07	0.07	0.07	0.07	5.99
MgO	0.90	0.61	1.01	0.70	0.56	1.60	0.90	1.01	0.95	0.82	0.85	0.11
FeO	2.37	2.39	2.69	2.03	2.30	2.93	2.37	2.54	2.46	2.49	2.56	3.92
CaO	2.47	2.14	2.23	2.16	1.93	3.88	3.25	3.18	2.99	2.81	2.79	7.94
Na_2O	5.62	4.49	4.35	4.37	4.62	4.23	4.97	4.58	4.57	4.53	4.56	3.65
K_2O	3.02	3.01	3.23	3.36	3.57	2.80	2.74	2.97	2.93	3.12	3.06	1.41
P_2O_5	0.03	0.05	0.07	0.09	0.08	0.09	0.09	0.09	0.08	0.08	0.09	0.15
Total	94.01	95.14	95.31	97.50	95.61	96.27	97.18	96.54	97.32	96.38	96.38	98.32
LOI	5.15	4.14	3.83	1.75	3.01	2.60	2.37	2.48	2.34	2.61	2.84	0.80
Ba	819	772	723	844	777	688	748	739	766	762	760	350
Ce	46	54	63	49	56	46	50	53	51	56	54	42
La	29	33	36	31	33	30	31	33	36	34	36	23
Nb	14.7	15.1	16.7	15.5	16.4	12.9	13.1	13.2	13.9	14.0	14.1	10.5
Nd	15.8	20.9	24.5	18.2	19.9	19.4	18.9	20.1	20.2	19.8	21.6	21.9
Rb	83	86	92	97	94	79	82	84	88	89	91	32
Sr	227	195	201	229	188	315	284	281	270	258	266	564
Th	9.7	10.5	11.0	12.8	11.8	9.2	10.2	10.3	10.8	10.9	10.8	2.6
U	2.9	3.5	3.0	3.9	3.7	2.9	3.1	2.5	3.3	3.3	2.8	<0.8
Y	16	16	20	14	18	17	15	16	17	16	17	22
Zr	241	243	253	154	259	199	199	206	203	206	210	158

In addition, inter-laboratory and calibration differences and, in particular, differences in analytical method may also account for some of the apparent variability within, and the resultant overlap between, Lower and Upper Pumice whole rock data.

Fig. 8 compares our proximal glass data for Lower and Upper Pumice samples to whole rock XRF data for the same pumice samples. Relative to the glass data, the whole rock data for both the Lower Pumice and Upper Pumice lie at less evolved compositions with 70.5–72.6 and 68.2–70.6 wt.% SiO_2 respectively. This implies that the Lower Pumice is more evolved, but the glass data indicate that the reverse is true. The largest deviation between whole rock and glass data occurs for elements which are compatible in plagioclase (Sr, Na_2O), Fe–Ti oxides, zircon (Zr) and clinopyroxene (MgO, FeO, CaO, V). The glass is enriched by $\leq 1.8\times$ the whole rock concentration of elements which are not compatible in these minerals. The differences between glass and whole rock data can be accounted for by inclusion of approximately 23% and 27% plagioclase in the Lower and Upper Pumice respectively, in addition to ~1% titano-magnetite and 2% clinopyroxene in the analysed whole rock samples (calculated using the partition coefficients of Arth (1976)). The effect of phenocrysts on the magma composition determined by whole rock techniques is extreme for the Lower and Upper Pumice because these are particularly phenocryst-rich and because of variations in the abundance and mineralogy of individual pumices. Margari et al.

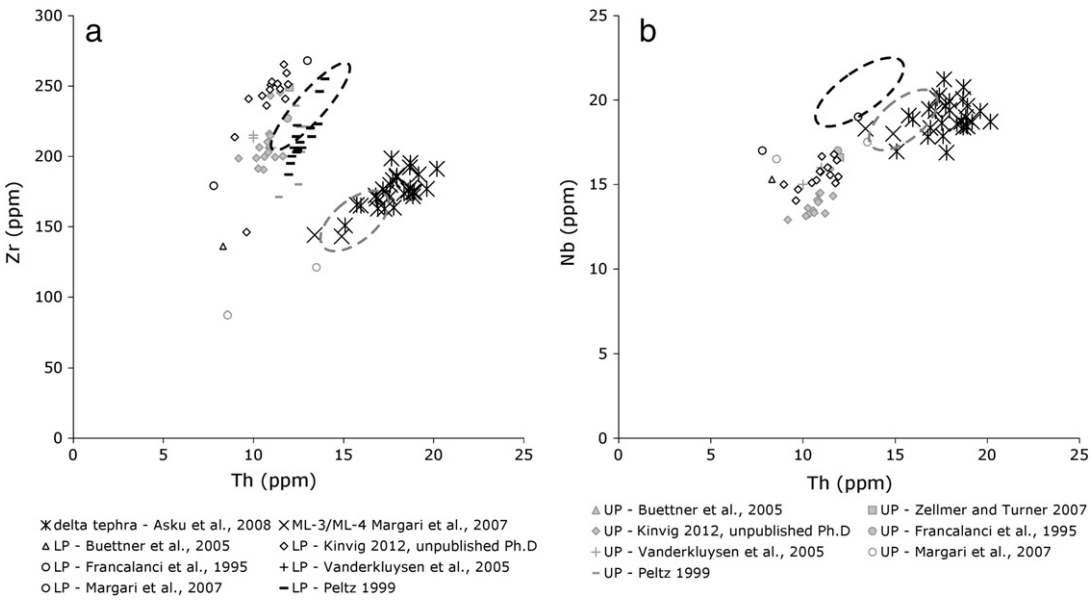

Fig. 7. Trace element biplots showing published whole rock data for the Lower (small black symbols) and Upper Pumice (small grey symbols) and for the distal (large symbols) delta tephra (Aksu et al., 2008) and ML-3/ML-4 tephra (Margari et al., 2007). Also shown is the field of Lower (black dashed line) and Upper (grey dashed line) glass compositions from this study.

Author's personal copy

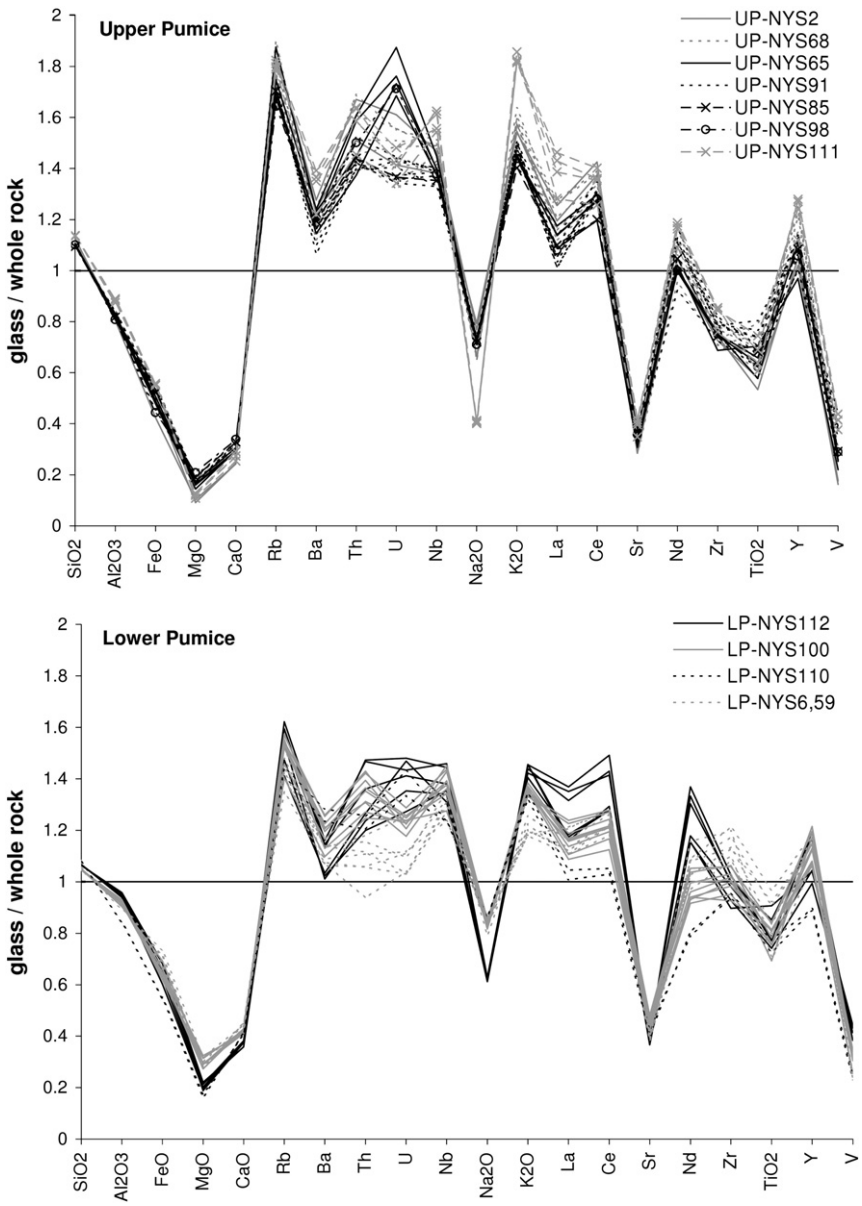

Fig. 8. Composition of Upper and Lower Pumice glass normalised to the whole rock composition of the equivalent sample. Major element compositions are normalised to 100% in both glass and whole rock data.

(2007) recognized that whole rock data may be compromised by included phenocrysts and so prepared fine sieve fractions of pure glass from proximal Lower and Upper Pumice samples for analysis by ICP-MS. However, when compared to the LA-ICP-MS glass data for proximal samples (this study) and distal samples (the delta tephra; Aksu et al., 2008), the ICP-MS data presented by Margari et al. (2007) has smaller Sr, Ba and Eu anomalies consistent with plagioclase inclusion, and also has a range of Zr contents suggesting variable inclusion (and possibly dissolution) of zircon.

In contrast to proximal tephra, distal ashes are typically more pure because crystals are not transported as far from the vent. In order to recognize these distal tephra, equivalent scale (micron-beam) glass data is needed for candidate proximal deposits. We therefore recommend the use of proximal trace element datasets comprising micron-beam glass data (LA-ICP-MS or SIMS) for tephrostratigraphic correlations. There is currently a paucity of such data in the literature. The NERC RESET project aims to rectify this problem by producing a database of European volcanic glass compositions for tephrostratigraphy (c14.arch.ox.ac.uk/reset).

5.3. Age and size of the Nisyros Lower and Upper Pumice eruptions

Tephra layers in sedimentary cores provide important constraints on the age, order and magnitude of volcanic eruptions.

5.3.1. Upper Pumice

Nisyros Upper Pumice tephra lies below Campanian Ignimbrite tephra in Aegean marine cores (Aksu et al., 2008), constraining its age to older than 39.3 ± 0.1 ka (De Vivo et al., 2001). Aksu et al. (2008) estimate an age of 42–44 ka for the delta tephra, here recognized as the Nisyros Upper Pumice, by linear extrapolation of oxygen isotope stratigraphy. This is comparable to the age of 46.8 ± 5.7 ka cal yr for the first occurrence of Upper Pumice tephra in the Lesvos core, determined from a combined radiocarbon and tephrochronology age model (Margari et al., 2007). This distal age estimate is consistent with the >47.7 cal ka BP age of the Upper Pumice obtained on charcoal in the proximal deposit (Limburg and Varekamp, 1991; calibrated using the IntCal09 calibration curve of Reimer et al. (2009)) and with its stratigraphic occurrence below

Author's personal copy

the ca. 31 ka Yali deposits (Federman and Carey). Therefore, the age of the Upper Pumice of Nisyros is ca. 47 ka.

The Lesvos core contains two Nisyros tephras, ML-4 and ML-3 dated at 46.8 ± 5.7 and 46.0 ± 5.7 ka cal yr BP, respectively. ML-3 and ML-4 were originally interpreted as the Lower and Upper Pumice events (Margari et al., 2007), however comparison with our proximal data strongly indicate that ML-4 and ML-3 both represent the Upper Pumice. The ML-3 and ML-4 tephra layers are separated by 1.3 m in the Lesvos core, both layers lack the normal sorting seen in marine cores and show a pattern of increasing sand upward, which is attributed inwashing of material from the catchment slopes (Margari et al., 2007). Visual and X-ray analysis does not show evidence of slumping or reworking tephra, therefore Margari et al. (2007) interpret ML-4 and ML-3 as two primary volcanic layers, even thought the glasses are compositionally identical. This would imply that the Upper Pumice was deposited during two eruptions closely spaced in time, forming two layers in the Lesvos core. However, there is no clear proximal evidence for more than one Upper Pumice eruption.

The presence of Upper Pumice ash in the Lesvos core, 300 km north of Nisyros, confirms the northerly dispersal of this eruption (Hardiman, 1999; Longchamp et al., 2011). The presence of the tephra in the Lesvos cores to the N (Margari et al., 2007), and the 7 cm thickness of the Upper Pumice in the MC27 core (Vinci, 1985), 120 km SW of Nisyros, are inconsistent with the estimated Upper Pumice volumes of Hardiman (1999) and Longchamp et al. (2011). Comparisons with other eruptions, which produced a similar deposit thinning at this distance from the vent (~10 cm at ~110 km), imply that the volume must be >2 km^3 with a VEI of ~5 (e.g., the eruption of Hudson 1991 had a similar column height and similar proximal and distal thicknesses; Scasso et al., 1994; Bonadonna and Costa, 2012). This is comparable to the 2–3 km^3 estimated using proximal and distal tephra thicknesses (Limburg and Varekamp, 1991). However, this assumes that the 7 cm thickness in MC27 is primary and not reworked; in core MAR03-28 the Upper Pumice layer is 13 mm thick but is impure and burrow mixed (Aksu et al., 2008).

5.3.2. Lower Pumice

The age of the Lower Pumice is constrained to between 161 and 47 ka by the Kos Plateau Tuff (Smith et al., 1996) and the Upper Pumice (Margari et al., 2007). However, the apparent absence of a paleosol between the Lower and Upper Pumice may imply a shorter age gap. The Lower Pumice has not been dated proximally and is not found in distal settings.

There are several possible explanations for the absence of the Lower Pumice in distal settings in which the Upper Pumice is preserved. One possibility is that the Lower Pumice is significantly older than the Upper Pumice and is beyond the age range of distal sedimentary records. The Lesvos core extends to ~62 ka (Margari et al., 2007) while Aegean marine cores contain the X1 tephra (Aksu et al., 2008) dated at 70 ka (Keller et al., 1978). Therefore, this scenario requires that the Lower Pumice is older than ~70 ka.

The second is that the Lower Pumice may have followed a different dispersal axes. Proximal mapping indicates that the Lower Pumice was distributed in a slightly more easterly direction (NE or NNE; Hardiman, 1999; Longchamp et al., 2011) than the Upper Pumice (NNE or N-NW; Hardiman, 1999; Longchamp et al., 2011), which may explain the absence of the Lower Pumice in distal settings to the N and NNE of Nisyros. In both scenarios, the Lower Pumice tephra may be present as a crypto horizon below the Upper Pumice in Lesvos and the Aegean Sea and this may provide the best opportunity to obtain an age for the Lower Pumice eruption of Nisyros.

6. Conclusions

Our new proximal dataset show that the Lower and Upper Pumice of Nisyros can be clearly distinguished on the basis of both major and trace element glass analyses. We have re-examined distal occurrences of Nisyros tephra from marine and terrestrial cores. Our new data supports the original interpretation that these tephras originated from Nisyros. However we show that all of these distal tephra were produced during the eruption of the Upper Pumice and not the Lower Pumice with which they were originally correlated. Based on the concordance between the Upper Pumice proximal ^{14}C age of Limburg and Varekamp (1991), the oxygen isotope stratigraphy age of Aksu et al. (2008) and the model age of ML-4 (Margari et al., 2007) we suggest an age of at least 47 ka for the Upper Pumice. The older Lower Pumice has not been found in distal records and its age is not well constrained. High-quality major and trace element glass datasets of proximal volcanic deposits are keys to correlating distal Nisyros tephra.

Acknowledgements

The authors are grateful to Ali Aksu for making available the full dataset of delta tephra compositions. We would like to thank Judy Fierstein and an anonymous reviewer for helpful comments. This work is funded by the NERC RESET consortium (NE/E015905/1). This is paper number ROX/0023. HK acknowledges NERC studentship (NE/F007299/1). JG was supported by funds from the Royal Society (URF) and the NERC (NE/E007961/1).

Appendix A. Supplementary data

Supplementary data to this article can be found online at http://dx.doi.org/10.1016/j.jvolgeores.2012.07.004.

References

Aksu, A.E., Jenner, G., Hiscott, R.N., Isler, E.B., 2008. Occurrence, stratigraphy and geochemistry of Late Quaternary tephra layers in the Aegean Sea and the Marmara Sea. Marine Geology 252 (3–4), 174–192.

Arth, J.G., 1976. Behavior of trace-elements during magmatic processes — summary of theoretical models and their applications. Journal of Research of the U. S. Geological Survey 4 (1), 41–47.

Bachmann, O., Schoene, B., Schnyder, C., Spikings, R., 2010. The Ar-40/Ar-39 and U/Pb dating of young rhyolites in the Kos-Nisyros volcanic complex, Eastern Aegean Arc, Greece: age discordance due to excess Ar-40 in biotite. Geochemistry, Geophysics, Geosystems 11, Q0AA08.

Barberi, F., Navarro, J.M., Rosi, M., Santacroce, R., Sbrana, A., 1988. Explosive interaction of magma with ground water: insights from xenoliths and geothermal drillings. Rendiconti della Societa Italiana di Mineralogica e Petrologica 43, 901–926.

Bonadonna, C., Costa, A., 2012. Estimating the volume of tephra deposits: a new simple strategy. Geology 1–5, http://dx.doi.org/10.1130/G32769.1.

Borchardt, G.A., Harward, M.E., Schmitt, R.A., 1971. Correlation of volcanic ash deposits by activation analysis of glass separates. Quaternary International 1 (2), 247–260.

Buettner, A., Kleinhanns, I.C., Rufer, D., Hunziker, J.C., Villa, I.M., 2005. Magma generation at the easternmost section of the Hellenic arc: Hf, Nd, Pb and Sr isotope geochemistry of Nisyros and Yali volcanoes (Greece). Lithos 83 (1–2), 29–46.

Caliro, S., et al., 2005. Recent activity of Nisyros volcano (Greece) inferred from structural, geochemical and seismological data. Bulletin of Volcanology 67 (4), 358–369.

De Vivo, B., et al., 2001. New constraints on the pyroclastic eruptive history of the Campanian volcanic Plain (Italy). Mineralogy and Petrology 73 (1–3), 47–65.

Di Paola, G., 1974. Volcanology and petrology of Nisyros Island (Dodecanese, Greece). Bulletin of Volcanology 38, 944–987.

Drouza, S., Georgoulias, F.A., Moustakas, N.K., 2006. Investigation of soils developed on volcanic materials in Nisyros Island, Greece. Catena 70, 340–349.

Federman, A.N., Carey, S.N., 1980. Electron microprobe correlation of tephra layers from Eastern Mediterranean abyssal sediments and the Island of Santorini. Quaternary Research 13 (2), 160–171.

Francalanci, L., et al., 1995. Crystal retention, fractionation and crustal assimilation in a convecting magma chamber, Nisyros Volcano, Greece. Bulletin of Volcanology 56 (8), 601–620.

Francalanci, L., Vougioukalakis, G.E., Perini, G., Manetti, P., 2005. A west–east traverse along the magmatism of the south Aegean volcanic arc in the light of volcanological, chemical and isotope data, South Aegean Active Volcanic Arc: present knowledge and future perspectives. Developments in Volcanology, Amsterdam, pp. 65–111.

Gottsmann, J., Carniel, R., Coppo, N., Wooller, L., Hautman, S., Rymer, H., 2007. Oscillations in hydrothermal systems as a source of periodic unrest at caldera volcanoes: multiparameter insights from Nisyros, Greece. Geophysical Research Letters 34, L07307.

Author's personal copy

Hardiman, J.C., 1996. Quaternary Volcanism on Nisyros, Greece. Ph.D Thesis, University of Cambridge, Cambridge, 336 pp.
Hardiman, J.C., 1999. Deep sea tephra from Nisyros Island, eastern Aegean Sea, Greece. In: Firth, C.R., McGuire, W.J. (Eds.), Volcanoes in the Quaternary: Geological Society of London, Special Publication, pp. 69–88.
Jochum, K.P., et al., 2006. MPI-DING reference glasses for in situ microanalysis: new reference values for element concentrations and isotope ratios. Geochemistry, Geophysics, Geosystems 7 (Q02008), 45.
Keller, J., Ryan, W.B.F., Ninkovich, D., Altherr, R., 1978. Explosive volcanic activity in the Mediterranean over the past 200,000 yr as recorded in deep-sea sediments. Geological Society of America Bulletin 89 (4), 591–604.
Keller, J., Gillot, P.Y., Rehren, T., Stadkbauer, E., 1989. Chronostratigraphic data for the volcanism in the eastern Hellenic Arc: Nisyros and Kos. Terra Abstracts 1, 354.
Lagios, E., Sakkas, V., Parcharidis, I., Dietrich, V., 2005. Ground deformation of Nisyros Volcano (Greece) for the period 1995–2002: results from DInSAR and DGPS observations. Bulletin of Volcanology 68, 201–214.
Le Maitre, R.W., et al., 1989. A classification of igneous rocks and glossary of terms: recommendations of the International Union of Geological Sciences Subcommission on the Systematics of Igneous Rocks. Blackwell Scientific Publications, Oxford, U.K.
Limburg, E.M., Varekamp, J.C., 1991. Young pumice deposits on Nisyros, Greece. Bulletin of Volcanology 54 (1), 68–77.
Longchamp, C., Bonadonna, C., Bachmann, O., Skopelitis, A., 2011. Characterisation of tephra deposits with limited exposure: the example of the two largest explosive eruptions at Nisyros volcano (Greece). Bulletin of Volcanology 73, 1337–1352.
Lowe, J.J., et al., 2007. Age modelling of late Quaternary marine sequences in the Adriatic: towards improved precision and accuracy using volcanic event stratigraphy. Continental Shelf Research 27 (3–4), 560–582.
Margari, V., Pyle, D.M., Bryant, C., Gibbard, P.L., 2007. Mediterranean tephra stratigraphy revisited: results from a long terrestrial sequence on Lesvos Island, Greece. Journal of Volcanology and Geothermal Research 163 (1–4), 34–54.
Marini, L., et al., 1993. Hydrothermal eruptions of Nisyros (Dodecanese, Greece), past events and present hazard. Journal of Volcanology and Geothermal Research 56 (1–2), 71–94.
Müller, W., Shelley, M., Miller, P., Broude, S., 2009. Initial performance metrics of a new custom-designed ArF excimer LA-ICPMS system coupled to a two-volume laser-ablation cell. Journal of Analytical Atomic Spectrometry 24 (2), 209–214.
Paterne, M., Guichard, F., Labeyrie, J., 1988. Explosive activity of the South Italian volcanoes during the past 80,000 years as determined by marine tephrochronology. Journal of Volcanology and Geothermal Research 34 (3–4), 153–172.
Peltz, C., Schmid, P., Bichler, M., 1999. INAA of Aegaean pumices for the classification of archaeological findings. Journal of Radioanalytical and Nuclear Chemistry 242 (2), 361–377.
Perkins, M.E., Nash, W.P., Brown, F.H., Fleck, R.J., 1995. Fallout tuffs of Trapper Creek, Idaho: a record of Miocene explosive volcanism in the Snake River Plain volcanic province. Geological Society of America Bulletin 107 (12), 1484–1506.
Pichon, X.L., Angelier, J., 1979. The Hellenic arc and trench system: a key to the neotectonic evolution of the eastern Mediterranean area. Tectonophysics 60 (1–2), 1–42.
Reimer, P.J., Baillie, M.G.L., Bard, E., Bayliss, A., Beck, J.W., Blackwell, P.G., Bronk, Ramsey C., Buck, C.E., Burr, G.S., Edwards, R.L., Friedrich, M., Grootes, P.M., Guiderson, T.P., Hajdas, I., Heaton, T.J., Hogg, A.G., Hughen, K.A., Kaiser, K.F., Kromer, B., McCormac, F.G., Manning, S.W., Richards, D.A., Southon, J.R., Talamo, S., Turney, C.S.M., van der Plicht, J., Weyhenmeyer, C.E., 2009. IntCal09 and Marine09 radiocarbon age calibration curves, 0–50,000 years cal BP. Radiocarbon 51 (4), 1111–1150.
Rehren, T., 1988. Geochemie und Petrologie von Nisyros (Ofstliche Agais). Ph.D thesees. Dept. of Geol., Univ. of Freiburg, Freiburg, Germany.
Saminger, S., Peltz, C., Bichler, M., 2000. South Aegean volcanic glass: separation and analysis by INAA and EPMA. Journal of Radioanalytical and Nuclear Chemistry 245 (2), 375–383.
Scasso, R.A., Corbella, H., Tineri, P., 1994. Sedimentological analysis of the tephra from the 12–15 August 1991 eruption of Hudson Volcano. Bulletin of Volcanology 56, 121–132.
Smith, P.E., York, D., Chen, Y., Evensen, N.M., 1996. Single crystal ^{40}Ar–^{39}Ar dating of a Late Quaternary paroxysm on Kos, Greece: concordance of terrestrial and marine ages. Geophysical Research Letters 23 (21), 3047–3050.
St.Seymour, K., Vlassopoulos, D., 1992. Magma mixing at Nisyros Volcano, as inferred from incompatible trace-element systematics. Journal of Volcanology and Geothermal Research 50 (3), 273–299.
Sun, S.-S., McDonough, W.F., 1989. Chemical and isotopic systematics of oceanic basalts: implications for mantle composition and processes. In: Saunders, A.D., Norry, M.J. (Eds.), Magmatism in Ocean Basins: Geological Society of London Special Publication, London, pp. 313–345.
Tomlinson, E.L., Thordarson, T., Muller, W., Thirlwall, M., Menzies, M.A., 2010. Micro analysis of tephra by LA-ICP-MS — strategies, advantages and limitations assessed using the Thorsmork ignimbrite (Southern Iceland). Chemical Geology 279 (3–4), 73–89.
Vanderkluysen, L., Volentik, A.C.M., Principe, C., Hunziker, J.C., Hernandez, J., 2005. Nisyros' volcanic evolution: the growth of a stratovolcano. In: Marini, J.C.H.a.L. (Ed.), The Geology, Geochemistry and Evolution of Nisyros Volcano (Greece), Implications for the Volcanic Hazards. Mémoires de Géologie, Lausanne.
Vinci, A., 1985. Distribution and chemical composition of tephra layers from Eastern Mediterranean abyssal sediments. Marine Geology 64 (1–2), 143–155.
Volentik, A., Vanderkluysen, L., Principe, C., 2002. Stratigraphy of the Caldera walls of Nisyros volcano, Greece. Eclogae Geologicae Helvetiae 95 (2), 223–235.
Wulf, S., Kraml, M., Brauer, A., Keller, J., Negendank, J.F.W., 2004. Tephrochronology of the 100 ka lacustrine sediment record of Lago Grande di Monticchio (southern Italy). Quaternary International 122, 7–30.
Wyers, G.P., Barton, M., 1989. Polybaric evolution of calc-alkaline magmas from nisyros, southeastern hellenic arc, Greece. Journal of Petrology 30 (1), 1–37.
Zellmer, G.F., Turner, S.P., 2007. Arc dacite genesis pathways: evidence from mafic enclaves and their hosts in Aegean lavas. Lithos 95 (3–4), 346–362.